The Company of Biologists

RESEARCH ARTICLE

The MAPK Erk5 is necessary for proper skeletogenesis involving a Smurf-Smad-Sox9 molecular axis

Takashi Iezaki[1,2,*], Kazuya Fukasawa[1,*], Tetsuhiro Horie[1,*], Gyujin Park[1], Samuel Robinson[3], Michio Nakaya[4], Hiroyuki Fujita[1], Yuki Onishi[1], Kakeru Ozaki[1], Takashi Kanayama[1], Manami Hiraiwa[1], Yuka Kitaguchi[1], Katsuyuki Kaneda[1], Yukio Yoneda[5], Takeshi Takarada[6], X. Edward Guo[3], Hitoshi Kurose[4] and Eiichi Hinoi[1,‡]

ABSTRACT

Erk5 belongs to the mitogen-activated protein kinase (MAPK) family. Following its phosphorylation by Mek5, Erk5 modulates several signaling pathways in a number of cell types. In this study, we demonstrated that Erk5 inactivation in mesenchymal cells causes abnormalities in skeletal development by inducing Sox9, an important transcription factor of skeletogenesis. We further demonstrate that Erk5 directly phosphorylates and activates Smurf2 (a ubiquitin E3 ligase) at Thr[249], which promotes the proteasomal degradation of Smad proteins and phosphorylates Smad1 at Ser[206] in the linker region known to trigger its proteasomal degradation by Smurf1. Smads transcriptionally activated the expression of Sox9 in mesenchymal cells. Accordingly, removal of one *Sox9* allele in mesenchymal cells from Erk5-deficient mice rescued some abnormalities of skeletogenesis. These findings highlight the importance of the Mek5-Erk5-Smurf-Smad-Sox9 axis in mammalian skeletogenesis.

KEY WORDS: MAPK, Smads, Smurfs, Sox9, Proteasomal degradation, Skeletal development, Mouse

INTRODUCTION

Extracellular signal-regulated kinase 5 (Erk5; Mapk7 – Mouse Genome Informatics) is a member of the mitogen-activated protein kinase (MAPK) family, which includes Erk1 (Mapk3), Erk2 (Mapk1), c-Jun amino-terminal kinase (Mapk8/9) and p38 (Mapk14) (Robinson and Cobb, 1997; Chang and Karin, 2001; Raman et al., 2007). Erk5 is specifically phosphorylated and activated by MAPK/Erk kinase 5 (Mek5; Map2k5) (English et al., 1995; Zhou et al., 1995), and *Erk5* knockout is embryonically lethal in mice owing to multiple developmental defects (Regan et al., 2002; Yan et al., 2003). Erk1 and Erk2 exhibit a high degree of similarity, and they are considered functionally equivalent, although isoform-specific differences have been described (Robinson and

Cobb, 1997). Erk5 has a larger molecular mass than other Erks (approximately 2-fold larger than Erk1/2) owing to a unique C-terminal extension that encodes two proline-rich regions and a nuclear localization signal (Buschbeck and Ullrich, 2005; Nishimoto and Nishida, 2006). Mouse genetic studies revealed that the Erk1/2 pathway plays an essential role in skeletal development by regulating successive steps associated with chondrocyte differentiation (Matsushita et al., 2009; Nithianandarajah-Jones et al., 2014; Chen et al., 2015). Moreover, mutations in signaling molecules of the Erk1/2 MAPK pathway also cause a number of human skeletal disorders, including Noonan, Costello and cardiofaciocutaneous syndromes (Bentires-Alj et al., 2006; Rodriguez-Viciana et al., 2006; Rauen, 2013). In contrast to Erk1/2, little is known about the role of Erk5 in skeletogenesis despite evidence for its physiological role in regulating a wide variety of cellular functions associated with vasculogenesis, angiogenesis and neurogenesis in different cell lineages (Regan et al., 2002; Sohn et al., 2002; Hayashi et al., 2004; Li et al., 2013).

Bone is formed by two distinct well-organized processes – intramembranous and endochondral ossification – during embryonic and postnatal skeletogenesis (Karsenty et al., 2009; Long and Ornitz, 2013). The flat bones of the skull, clavicle and mandible are ossified through intramembranous ossification, which involves the direct conversion of mesenchymal stem cells into osteoblasts to form bone (Long, 2012). Other bones, such as the long bones in the forelimbs (humerus, radius and ulna), hindlimbs (femur, tibia and fibula), and feet and hands (metatarsal, metacarpal and proximal phalanges), are formed by endochondral ossification (Johnson and Tabin, 1997). In endochondral ossification, mesenchymal stem cells differentiate into chondrocytes from a cartilaginous template. Chondrocytes differentiate, progressing through the resting, proliferating, hypertrophic and calcifying stages, leading to cartilage matrix mineralization around the central region of the rudiment in the area of hypertrophic chondrocytes. After mineralization, most hypertrophic chondrocytes undergo apoptosis, leading to the invasion of capillaries, osteoclasts, bone marrow cells and osteoblasts into the cartilage matrix to produce new bones (Kronenberg, 2003; Maes, 2013).

Paired-related homeobox 1 (Prx1; Prrx1) is expressed in mesenchymal cells in the limb buds and craniofacial mesenchyme (Cserjesi et al., 1992), and genetic research has revealed a crucial role for Erk1/2 in skeletogenesis through its expression in Prx1^{+}-derived cells (Matsushita et al., 2009). In this study, we demonstrated that Erk5 plays a pivotal role in skeletogenesis. In particular, we revealed its role in bone compartments, including the metatarsal, metacarpal and proximal phalanges, through its expression in Prx1^{+}-derived cells. Subsequent analyses uncovered that Erk5 directly phosphorylates Smad1 at Ser[206] in the linker region, which is known to trigger its proteasomal degradation in a

[1]Laboratory of Molecular Pharmacology, Division of Pharmaceutical Sciences, Kanazawa University Graduate School, Kanazawa, Ishikawa 920-1192, Japan. [2]Venture Business Laboratory, Organization of Frontier Science and Innovation, Kanazawa University, Kanazawa, Ishikawa 920-1192, Japan. [3]Bone Bioengineering Laboratory, Department of Biomedical Engineering, Columbia University, New York, NY 10027, USA. [4]Department of Pharmacology and Toxicology, Graduate School of Pharmaceutical Sciences, Kyushu University, Fukuoka 812-8582, Japan. [5]Section of Prophylactic Pharmacology, Venture Business Laboratory, Organization of Frontier Science and Innovation, Kanazawa University Kanazawa, Ishikawa 920-1192, Japan. [6]Department of Regenerative Science, Okayama University Graduate School of Medicine, Dentistry and Pharmaceutical Sciences, Okayama 700-8558, Japan.
*These authors contributed equally to this work

‡Author for correspondence (hinoi@p.kanazawa-u.ac.jp)

E.H., 0000-0002-1298-8293

DEVELOPMENT

1

Smad-specific E3 ubiquitin ligase 1 (Smurf1)-dependent manner. In addition, Erk5 directly phosphorylates Smurf2 at residue Thr^{249}, leading to the subsequent acceleration of the proteasomal degradation of Smad proteins (Smad1, Smad2 and Smad3). We demonstrated that Smads transcriptionally activate the expression of the sex-determining region within the Y-type high-mobility group box protein 9 (Sox9), which is the principal transcription factor of skeletogenesis in mesenchymal cells. Moreover, using mouse genetic rescue experiments, we revealed that Sox9 is a prominent mediator of Erk5-dependent skeletogenesis. Our results demonstrated that the Smurf-Smad-Sox9 axis is an important pathway through which Mek5-Erk5 signaling regulates skeletal development.

RESULTS

Mesenchymal-specific *Erk5* knockout mice display abnormal development of some long bones and the skull

To reveal the *in vivo* physiological role of Erk5 in skeletal development, we first generated mesenchymal-specific *Erk5* knockout mice using *Prx1-Cre* (Logan et al., 2002). Staining skeletal preparations from embryos at 18.5 days post-coitum (E18.5) with Alcian Blue and Alizarin Red indicated that the long bones in the forelimbs (humerus, radius and ulna) and hindlimbs (femur, tibia and fibula) were wider in *Prx1-Cre;Erk5$^{fl/fl}$* embryos (Fig. 1Aa-Ad, B), and a larger space was identified in the posterior fontanel (space between the parietal and interparietal bones) (Fig. 1Ae,Af). In addition, mineralization was impaired in metatarsal, metacarpal and proximal phalanges, but not in the femur and tibia, in *Prx1-Cre; Erk5$^{fl/fl}$* embryos at E18.5 (Fig. 1Ag-Aj, Fig. S1A).

Wider long bones (Fig. S1Cc-Cf, Fig. S2A-C) and defects of metatarsal mineralization (Fig. S1B,Ci-Cj) were also observed in *Prx1-Cre;Erk5$^{fl/fl}$* embryos at E16.5. Moreover, wider long bones were also observed in *Prx1-Cre;Erk5$^{fl/fl}$* embryos at E13.5 and E14.5 (Fig. S2A-C). In addition to femur and tibia, the width of the metatarsals was also increased in *Prx1-Cre;Erk5$^{fl/fl}$* embryos at E14.5, E16.5 and E18.5 (Fig. S2A,D).

Histological analyses also revealed a marked increase in long both width (Fig. 1C,D). In addition, almost all chondrocytes in the metatarsals of *Prx1-Cre;Erk5$^{fl/fl}$* embryos expressed collagen type II α1 (*Col2a1*), a marker of non-hypertrophic chondrocytes, whereas the middle portion of the metatarsals in control embryos did not express this marker (Fig. 1Eg,Eh). Moreover, the level of collagen type X (*Col10a1*), a hypertrophic chondrocyte marker, was reduced markedly in *Prx1-Cre;Erk5$^{fl/fl}$* embryos relative to control mice (Fig. 1Ei,Ej). These abnormalities in chondrocyte differentiation in the metatarsals were confirmed by Hematoxylin and Eosin (H&E) and Safranin O staining (Fig. 1Ea-Ed). Consistent with delays in chondrocyte hypertrophy and mineralization as determined by von Kossa staining, matrix metalloproteinase-13 (*Mmp13*) expression level was reduced in *Prx1-Cre;Erk5$^{fl/fl}$* embryos (Fig. 1Ee,Ef,Ek,El).

To examine further the physiological role of Erk5 in skeletal development *in vivo*, we generated cell-specific *Erk5* knockout mice using *Col2a1-Cre* and osterix (*Osx*; *Sp7*)-*Cre* drivers (Terpstra et al., 2003). Skeletal preparations and histological analyses revealed that *Col2a1-Cre;Erk5$^{fl/fl}$* embryos at E18.5 did not exhibit the abnormalities in space in the posterior fontanel or mineralization of the metatarsal, metacarpal and proximal phalanges noted in *Prx1-Cre;Erk5$^{fl/fl}$* embryos (Fig. S3A). However, these mutant mice recapitulated the wider long bone phenotype in the forelimbs and hindlimbs of *Prx1-Cre;Erk5$^{fl/fl}$* embryos at E18.5 (Fig. S2B,C, Fig. S3A-C). Moreover, wider long bones were also observed in *Col2a1-Cre;Erk5$^{fl/fl}$* embryos at E16.5 but not at E12.5, E13.5 or E14.5 (Fig. S2A-C).

Contrary to observations at embryonic stages, 3-week-old *Prx1-Cre;Erk5$^{fl/fl}$* mice displayed skeletal abnormalities, including deformities of the metatarsal bones in the feet and shorter and thinner long bones, whereas *Col2a1-Cre;Erk5$^{fl/fl}$* mice did not exhibit gross skeletal abnormalities at this age (Fig. S4A-C). Because the *Osx-Cre* transgene itself caused craniofacial bone development defects (Wang et al., 2015), we were unable to compare embryonic phenotypes in the space of the posterior fontanel between *Osx-Cre* and *Osx-Cre;Erk5$^{fl/fl}$* embryos. However, *Osx-Cre;Erk5$^{fl/fl}$* embryos did not exhibit abnormalities in metatarsal, metacarpal and proximal phalanx mineralization, nor did they affect the width of long bones in the forelimbs and hindlimbs relative to *Osx-Cre* embryos (Fig. S4D).

Collectively, among the phenotypic changes in Erk5-deficient mice generated by three different Cre drivers, the production of wider long bones was a common outcome following *Erk5* deletion by both *Prx1-Cre* and *Col2a1-Cre* drivers, whereas phenotypic changes involving a larger space in the posterior fontanel and impairment of mineralization of metatarsal, metacarpal and proximal phalanges were specific phenotypes related to *Erk5* deletion in Prx1$^+$ cells.

Erk5 controls chondrogenic differentiation of mesenchymal cells *in vitro*

To reveal whether skeletal abnormalities associated with Erk5 deficiency were derived from abnormalities in the chondrogenic differentiation of mesenchymal cells, micromass cultures of limb bud cells prepared from *Erk5$^{fl/fl}$* and *Prx1-Cre;Erk5$^{fl/fl}$* embryos were differentiated for 6 days and matured for 12 days, then stained with Alcian Blue and Alizarin Red. A marked increase in the size of the Alcian Blue-positive area was observed in Erk5-deficient cells at day 6, whereas the Alizarin Red intensity in the area was markedly decreased in Erk5-deficient cells at day 12 (Fig. 2A, Fig. S5A,B). In addition, the micromass diameter was significantly increased in Erk5-deficient cells at day 6 (Fig. S5C), suggesting that cell proliferation is altered in Erk5-deficient cells. In Erk5-deficient cells, significant increases were observed in the mRNA levels of *Col2a1*, aggrecan (*Acan*) and *Sox9* (Fig. 2B), whereas *Col10a1* and *Mmp13* levels were significantly decreased (Fig. 2C). Moreover, Sox9 protein levels were increased in Erk5-deficient cells despite no change in Runx2 and osterix levels (Fig. 2D).

We next investigated whether the Mek5-Erk5 pathway controlled the chondrogenic differentiation of mesenchymal cells *in vitro*. Alcian Blue-positive area and Alizarin Red intensity were inhibited by retroviral introduction of Erk5(WT) in control and Erk5-deficient cells (Fig. 2Ea-Ed,Eg-Ej). Erk5 phosphorylation was enhanced in cells infected with Erk5(WT) alone (Fig. 2F). In contrast, retroviral introduction of Erk5(DN) – the dominant-negative form of Erk5 that lacks the two phosphorylation sites for Mek5 and cannot phosphorylate target genes – led to an increase in the Alcian Blue-positive area and a decrease in the Alizarin Red intensity in control cells (Fig. 2Ea,Ee,Eg,Ek). This finding was consistent with previous observations in Erk5-deficient cells. No further changes in the differentiation and maturation of chondrocytes were noted when Erk5(DN) was introduced into Erk5-deficient cells (Fig. 2Eb,Ef,Eh,El). Moreover, retroviral introduction of Mek5D, the constitutively active form of Mek5, inhibited the differentiation and maturation of control cells but not Erk5-deficient cells (Fig. 2G).

In addition, CD45$^-$CD29$^+$Sca1$^+$CD105$^+$Ptprc$^+$Itgb$^+$Ly6a$^+$Eng$^+$ mesenchymal stem cells isolated from limb buds were subject to monolayer culture (2D micromass culture) and chondrogenic pellet
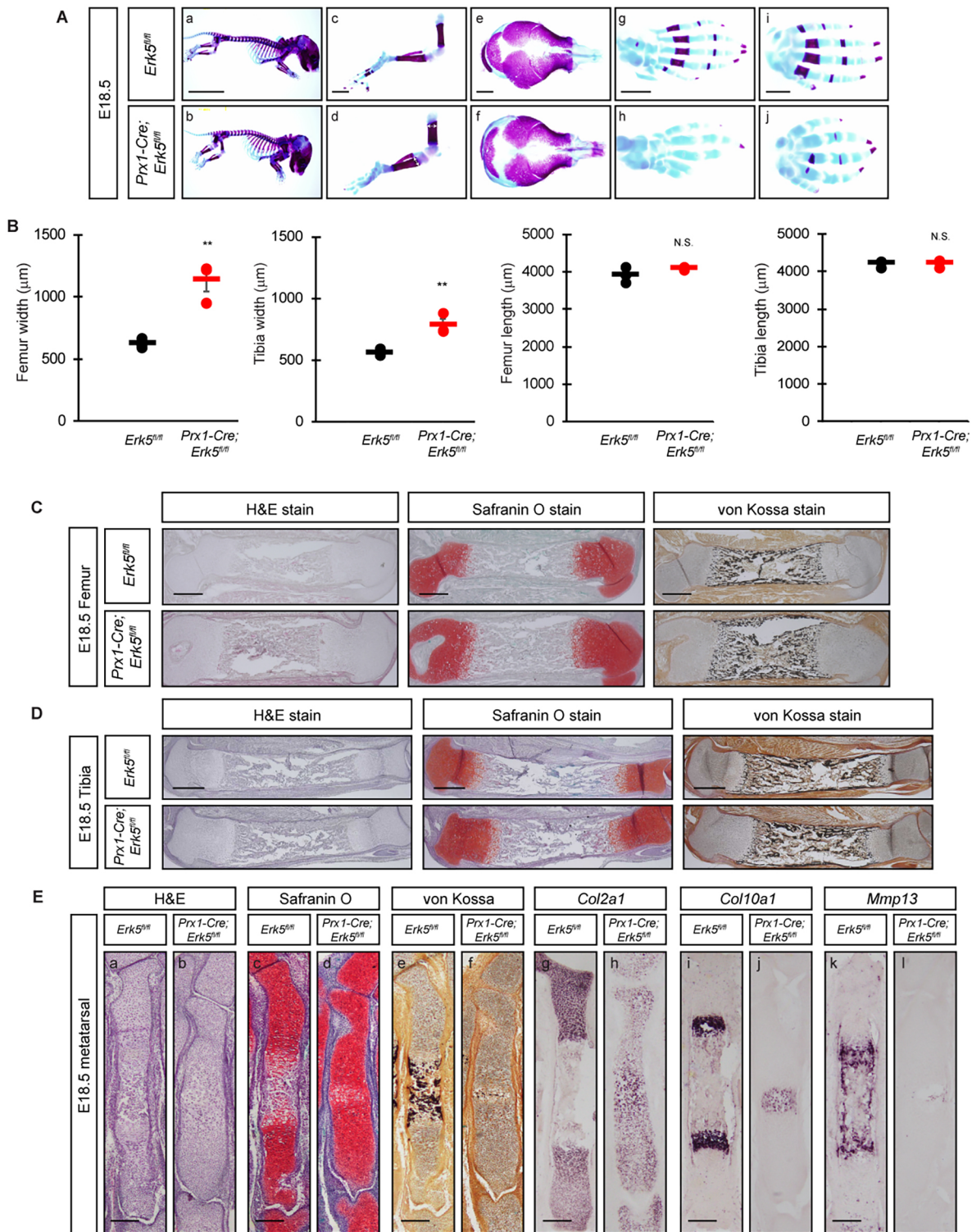
Fig. 1. Erk5 is essential for skeletogenesis *in vivo*. (A) The whole skeleton and parts of the skeleton at E18.5. Embryos were double stained with Alizarin Red and Alcian Blue. (B) Quantitative data of width (double-headed white arrows in Ad) and length of femur and tibia at E18.5 (*n*=3). (C,D) Histological analyses of the femur (C) and tibia (D) at E18.5. Femur and tibia were stained with H&E, Safranin O and von Kossa. (E) Histological and *in situ* hybridization analyses of the metatarsal at E18.5. Representative images of skeletal preparations and histological analyses derived from more than three embryos from different litters are shown. **$P<0.01$ (significantly different from the value obtained in control embryos; two-tailed, unpaired Student's *t*-test). N.S., not significant. Error bars represent s.e.m. Scale bars: 10 mm (Aa,Ab); 1 mm (Ac-Aj); 500 µm (C,D); 150 µm (E).

culture (3D pellet culture), followed by Alcian Blue staining (Fig. S5D). Alcian Blue staining was enhanced in Erk5-deficient CD45⁻CD29⁺Sca1⁺CD105⁺ mesenchymal stem cells (Fig. S5E), whereas the population of CD45⁻CD29⁺Sca1⁺CD105⁺ cells in the limb buds of *Prx1-Cre;Erk5^{fl/fl}* embryos was indistinguishable from that of control embryos (Fig. S5F).
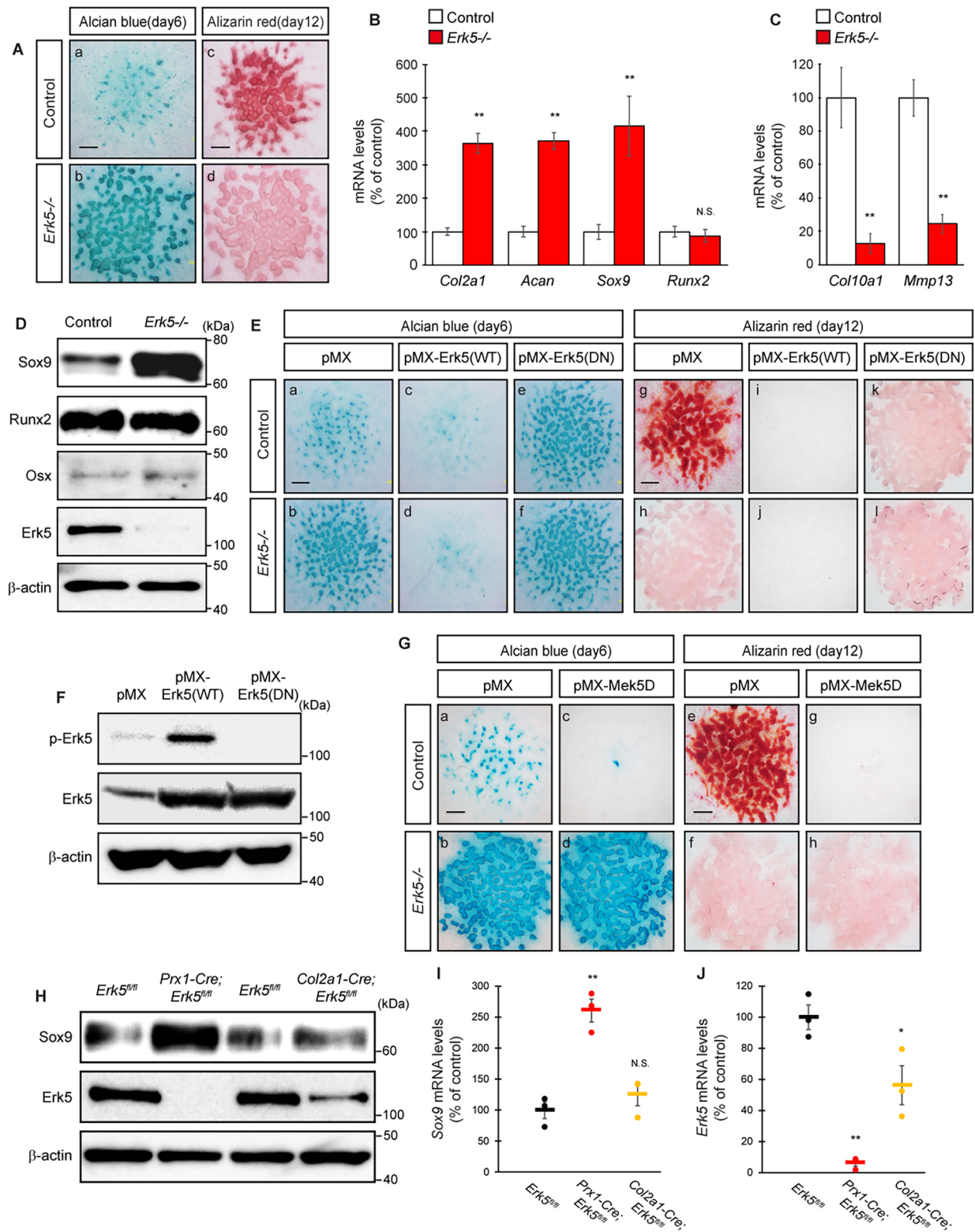
Fig. 2. Erk5 is essential for chondrogenesis *in vitro*. (A) Forelimb bud mesenchymal cells of *Erk5^fl/fl* (control) and *Prx1-Cre;Erk5^fl/fl* (*Erk5^−/−*) embryos at E12.5 were cultured, followed by Alcian Blue staining at day 6 (Aa,Ab) and Alizarin Red staining at day 12 (Ac,Ad) (*n*=5). (B-D) Primary mesenchymal cells were isolated from *Erk5^fl/fl* and *Prx1-Cre;Erk5^fl/fl* embryos at E12.5, and subsequently mRNA levels were determined by real-time quantitative PCR at day 6 (B) or day 12 (C) (*n*=5), and protein levels at day 6 (D) (*n*=3). (E,F) Primary mesenchymal cells were retrovirally infected with Erk5(WT) and Erk5(DN) expression vectors, followed by micromass culture, and subsequent Alcian Blue (Ea-Ef) and Alizarin Red (Eg-El) staining (*n*=5), and determination of protein levels (F) (*n*=3). (G) Primary mesenchymal cells were retrovirally infected with Mek5D expression vector, followed by micromass culture, and subsequent Alcian Blue staining at day 6 (Ga-Gd) and Alizarin Red staining at day 12 (Ge-Gh) (*n*=5). (H-J) Detection of Erk5 and Sox9 at protein (H) and mRNA (I,J) levels in forelimb buds of *Prx1-Cre; Erk5^fl/fl* and *Col2a1-Cre;Erk5^fl/fl* embryos at E12.5 (*n*=3). *P<0.05, **P<0.01 [significantly different from the value obtained in control cells (B,C) or control embryos (I,J); two-tailed, unpaired Student's *t*-test]. N.S., not significant. Error bars represent s.e.m. Scale bars: 500 μm (A,E,G).

Sox9 protein and mRNA levels were significantly increased in the forelimb buds of *Prx1-Cre;Erk5^fl/fl^* embryos but not *Col2a1-Cre;Erk5^fl/fl^* embryos (Fig. 2H,I, Fig. S5G). Erk5 protein and mRNA levels were significantly diminished in the forelimb buds of *Prx1-Cre;Erk5^fl/fl^* embryos, whereas their levels were significantly but modestly decreased in those of *Col2a1-Cre;Erk5^fl/fl^* embryos (Fig. 2H,J, Fig. S5H). Immunohistochemical analysis also revealed that Sox9 protein expression was markedly higher in the forelimb buds of *Prx1-Cre;Erk5^fl/fl^* embryos at E12.5 and the metatarsals at E16.5, whereas increased Sox9 expression was not detected in *Col2a1-Cre;Erk5^fl/fl^* embryos (Fig. S5I,J).

The Mek5-Erk5 pathway regulates ubiquitin-dependent Smad degradation

We next attempted to identify the factors responsible for altering the chondrogenic differentiation of mesenchymal cells and increasing Sox9 expression in Erk5-deficient cells. We monitored the activity of several reporters in Erk5-deficient cells. Among the tested reporters, BRE-luc (Smad1/5/8-dependent) and SBE4-luc (Smad2/3-dependent) displayed significantly increased expression in Erk5-deficient cells compared with controls (Fig. 3A). Consistent with the induction of Sox9 expression in Erk5-deficient cells (Fig. 2D), *Sox9* promoter activity (Sox9-luc) and Sox9-dependent transcriptional activity (4x48-luc) were increased significantly in Erk5-deficient cells, whereas no changes were noted in the *Runx2* promoter (Runx2-luc) or Runx2-dependent transcriptional activity (6xOSE2-luc) (Fig. 3A). We next attempted to elucidate the mechanism underlying the induction of Smad1/5/8- and Smad2/3-dependent transcriptional activities in Erk5-deficient cells. Smad mRNA levels were comparable between Erk5-deficient and control cells (Fig. 3B), whereas the protein levels of Smad1, Smad2 and Smad3, but not Smad5 or Smad8 (also known as Smad9), were increased in Erk5-deficient cells (Fig. 3C). Moreover, phosphorylation of Smad1/5/8 and Smad2 was increased in Erk5-deficient cells (Fig. 3C), in line with the results of the luciferase assays (Fig. 3A). Consistent with this finding, we observed that Smad1, Smad2 and Smad3 levels were elevated in the nuclei of Erk5-deficient cells along with the induction of Sox9 (Fig. 3D). These results suggest that Erk5 selectively regulates particular Smads at the protein, but not mRNA, level.

We next sought to elucidate whether Erk5 could selectively regulate Smad degradation. Erk5-deficient cells were treated with cycloheximide (CHX), a protein synthesis inhibitor, and Smad1, Smad2 and Smad3 levels were assayed. Smad1, Smad2 and Smad3 rapidly degraded in CHX-treated control cells, whereas their protein levels were more stable in Erk5-deficient cells (Fig. 3E, Fig. S6A-C). We next tested whether the Mek5-Erk5 pathway enhanced Smad1, Smad2 and Smad3 turnover through its ability to promote ubiquitylation. HA-tagged ubiquitin and Flag-tagged Smad1, Smad2 or Smad3 were co-introduced in the presence or absence of Mek5D and Erk5(WT) in HEK293 cells. In the absence of Mek5D and Erk5(WT), no ubiquitination was observed for any of the Smads examined. By contrast, ubiquitin-conjugated Smad products of high molecular weight (exceeding 80 kDa) were observed for Smad1, Smad2 and Smad3 in the presence of Mek5D and Erk5, whereas no high molecular weight products were observed when Mek5D and/or Erk5(WT) were transfected without Smads in HEK293 cells (Fig. 3F, Fig. S6D,E).

These results indicate that the Mek5-Erk5 pathway preferentially targets Smad1, Smad2 and Smad3 for ubiquitylation and proteasome-mediated degradation to regulate Smad1/5/8- and Smad2/3-dependent transcriptional activity.

Erk5 directly phosphorylates Smad1 at Ser^206^ in the linker region

To investigate the mechanism by which Mek5-Erk5 signaling stimulates the ubiquitylation and proteasome-mediated degradation of Smads, we examined whether Erk5 could phosphorylate and interact directly with Smad1, Smad2 and Smad3. An immunoprecipitation (IP) assay using recombinant proteins revealed that Erk5 directly interacted with Smad1 but not with Smad2 or Smad3 *in vitro* (IP with anti-Smad antibodies and probed with anti-Erk5 antibody) (Fig. 4A-C). Moreover, an *in vitro* kinase assay revealed that of the Smad proteins tested only Smad1 was phosphorylated by Erk5 (Fig. 4D-F).

Seven candidate serine or threonine sites in mouse Smad1 were identified from computer alignment with an optimal Erk5 substrate motif (Ser^11^, Ser^132^, Ser^187^, Ser^195^, Ser^206^, Ser^214^ and Ser^456^). To examine which candidate sites could be phosphorylated by Erk5, we generated seven site-directed mutant constructs of Smad1 (S11A, S132A, S187A, S195A, S206A, S214A and S456A), in which the serine was replaced by alanine to prevent phosphorylation. We then performed an *in vitro* kinase assay. Smad1 phosphorylation by Erk5(WT) was abolished by Smad1(S206A) but not by the other mutants (Fig. 4G). These results indicate that Erk5 directly phosphorylates Smad1 at Ser^206^, a residue known to be phosphorylated by Erk2, leading to the proteasomal degradation of Smad1 in a Smurf1-dependent manner (Sapkota et al., 2007).

Erk5 directly phosphorylates Smurf2 at Thr^249^ to activate Smad ubiquitylation, leading to the repression of chondrogenic differentiation

To investigate alternative mechanisms that could be involved in the ubiquitylation and proteasome-mediated degradation of Smads induced by the Mek5-Erk5 axis, we next investigated whether Erk5 could interact directly with Smurf2, another ubiquitin E3 ligase responsible for the ubiquitin-dependent degradation of Smads (Lin et al., 2000; Zhang et al., 2001). An IP assay revealed that Erk5 interacted with Smurf2 in HEK293 cells (IP with anti-Flag antibody and probed with anti-HA antibody), *in vitro* (cell-free system; IP with anti-Smurf2 antibody and probed with anti-Erk5 antibody) and in primary mesenchymal cells (IP with anti-Erk5 antibody and probed with anti-Smurf2 antibody) (Fig. 5A-C), indicating that Erk5 physically interacts with Smurf2.

Among the four candidate serine or threonine sites conserved in different species based on computer alignment to an optimal Erk5 substrate motif, one potential Erk5 phosphorylation site emerged in mouse Smurf2 at Thr^249^ (Fig. 5D, Fig. S7A). In addition, substrate sequence motifs indicated that Erk1/2 was unlikely to phosphorylate Smurf2 at Thr^249^ (Fig. S7A). To establish the role of this potential phosphorylation site in Smad degradation, we generated a site-directed mutant construct of Smurf2, Smurf2(T249A), in which the threonine was replaced by alanine to prevent phosphorylation. An *in vitro* kinase assay revealed that bacterially expressed recombinant Smurf2(WT) was phosphorylated by Erk5(active) but not by Erk5(inactive), whereas Smurf2 phosphorylation by Erk5 was stopped completely by Smurf2(T249A) (Fig. 5E), indicating that Erk5 directly phosphorylated Smurf2 at Thr^249^.

To investigate further the role of Smurf2 phosphorylation at Thr^249^ in Smad degradation, an *in vitro* ubiquitylation assay was performed with recombinant Smurf2(WT), Smurf2(T249A) and Smurf2(T249E), in which threonine was replaced with glutamate to mimic the phosphorylated state, as well as Erk5(active) and Smads. Incubation of Smurf2(WT) with ubiquitin, E1 and UbcH5c caused Smad protein ubiquitylation in the presence of Erk5 despite the
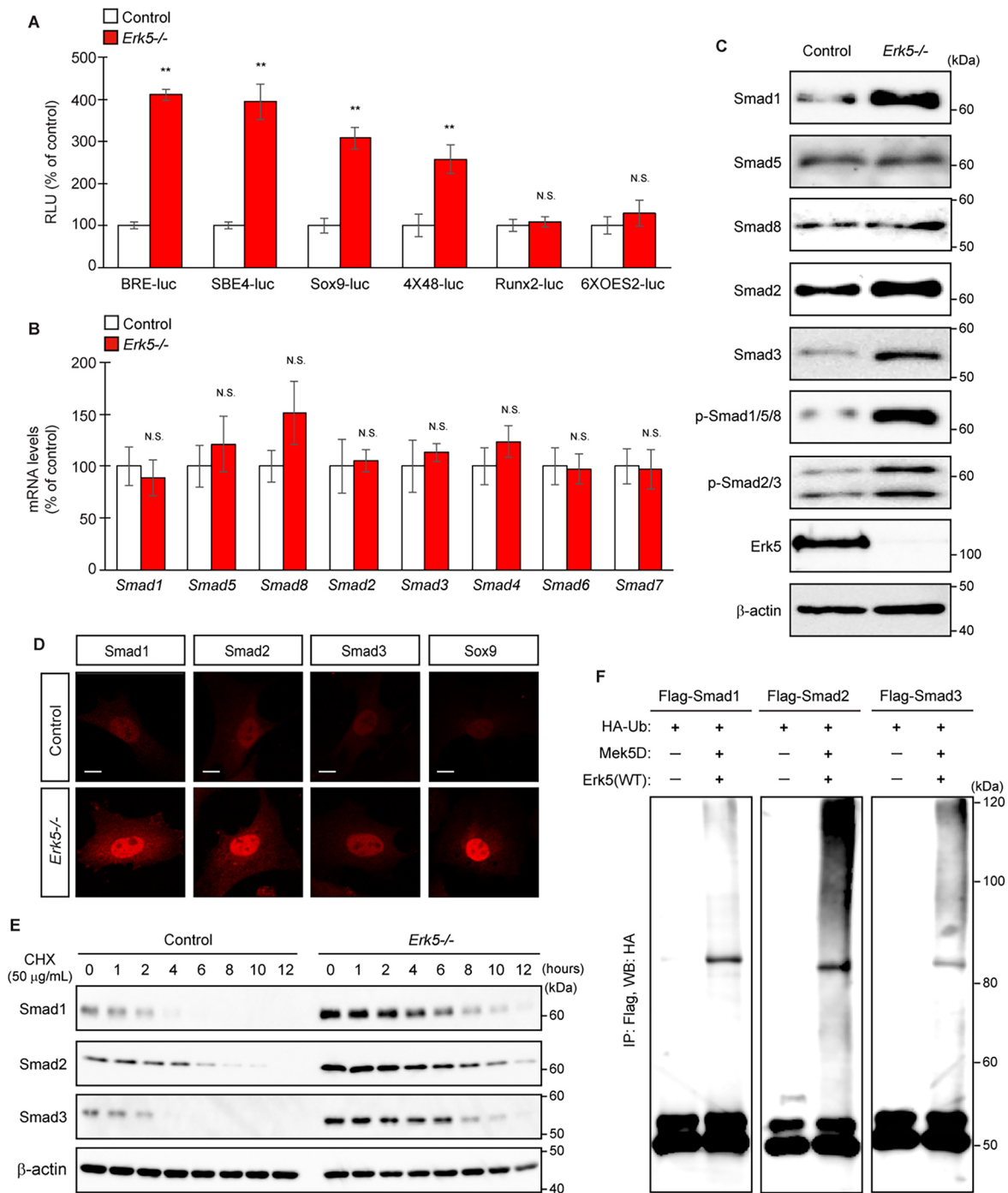
Fig. 3. Erk5 regulates ubiquitin-dependent degradation of Smad proteins. (A) Primary mesenchymal cells from *Erk5*^{fl/fl} (control) and *Prx1-Cre;Erk5*^{fl/fl} (*Erk5*^{−/−}) embryos at E12.5 were cultured for 1 day, and transiently transfected with various luciferase vectors (BRE-luc, SBE4-luc, Sox9-luc, 4x48-luc, Runx2-luc and 6xOSE2-luc) for determination of reporter activities (*n*=5). RLU, relative light unit. (B-D) Primary mesenchymal cells were isolated from *Erk5*^{fl/fl} and *Prx1-Cre;Erk5*^{fl/fl} embryos at E12.5, and subsequently mRNA levels were determined by qPCR (B) (*n*=5) and protein levels were determined by immunoblotting and immunocytochemistry (C,D) (*n*=3). (E) Primary mesenchymal cells from *Erk5*^{fl/fl} and *Prx1-Cre;Erk5*^{fl/fl} embryos were treated with cycloheximide at 50 µg/ml for the indicated number of hours, followed by immunoblotting (*n*=4). (F) HEK293 cells were transfected with HA-Ub and Flag-Smads in either the presence or absence of Mek5D and Erk5(WT) expression vectors. Subsequently, IP was performed with an anti-Flag antibody, followed by immunoblotting with anti-HA antibody (*n*=4). **$P<0.01$ (significantly different from the value obtained in control cells; two-tailed, unpaired Student's *t*-test). N.S., not significant. Error bars represent s.e.m. Scale bars: 10 µm.

weak ubiquitylation signal noted in the absence of Erk5. The reaction with Smurf2(T249A) produced a faint ubiquitylation signal in the presence of Smad1, Smad2 and Smad3, irrespective of the presence of Erk5, whereas extensive ubiquitylation was observed when Smads were incubated with Smurf2(T249E) in the absence of

Erk5. The addition of Erk5 did not increase ubiquitylation (Fig. 5F, Fig. S7B). Moreover, in the absence of Smad proteins, a faint ubiquitylation signal above 100 kDa was detected after adding Smurf2, irrespective of the presence or absence of Erk5, indicating ubiquitination of Smurf2 (Fig. S7C).
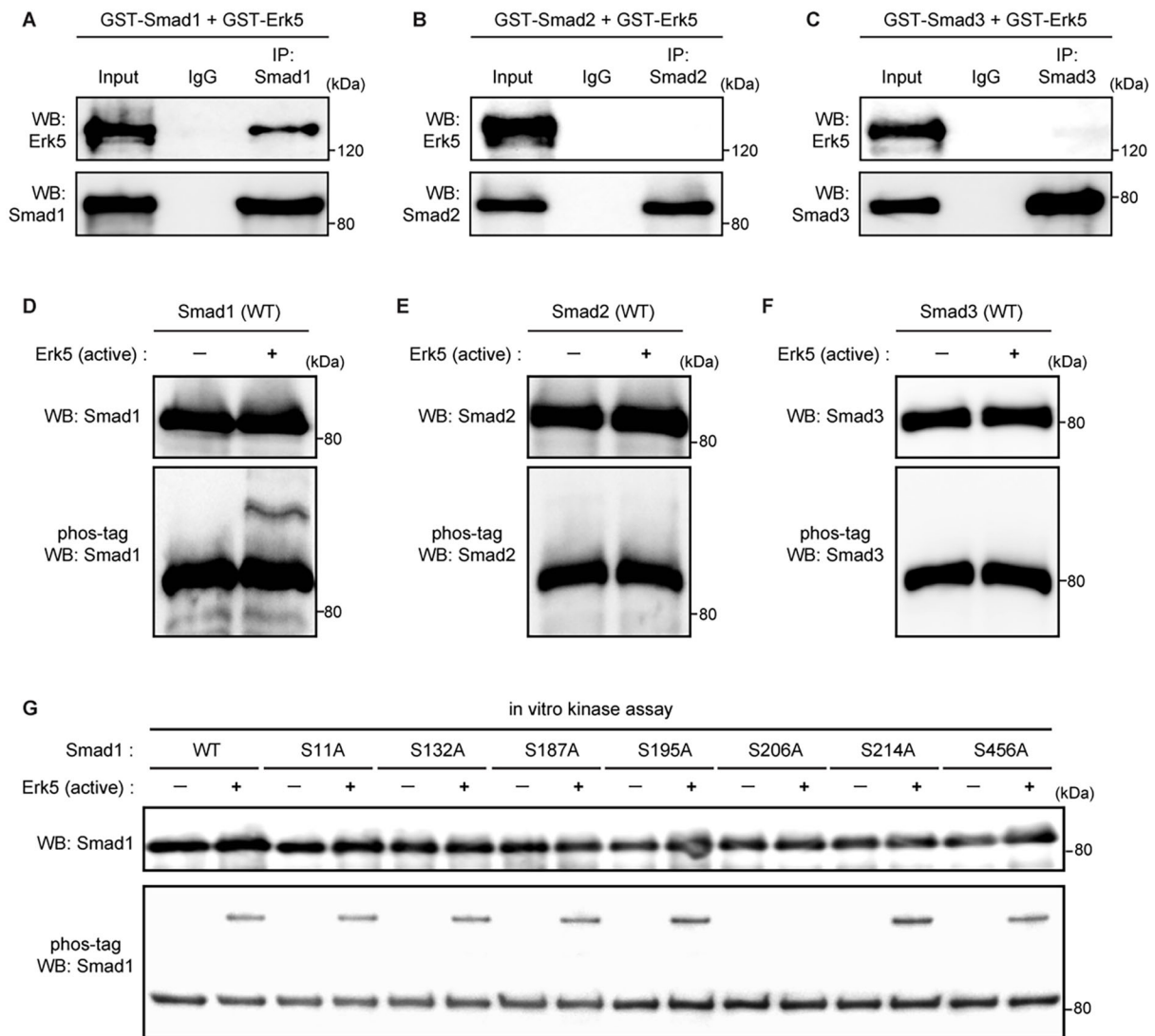
Fig. 4. Erk5 phosphorylates Smad1 at Ser[206] residue in the linker region. (A-C) IP assays were performed in a cell-free system with recombinant Smad1 (A), Smad2 (B) and Smad3 (C) proteins (*n*=3). (D-F) *In vitro* kinase assay. Recombinant Smad1(WT) (D), Smad2(WT) (E) and Smad3(WT) (F) proteins were incubated with active Erk5, followed by Phos-tag SDS-PAGE and subsequent immunoblotting (*n*=3). (G) *In vitro* kinase assay. Recombinant Smad1 proteins (WT and mutants) were incubated with active Erk5, followed by Phos-tag SDS-PAGE and subsequent immunoblotting (*n*=3).

Finally, we determined whether Smurf2 phosphorylation at Thr[249] was required for Erk5-dependent chondrogenic differentiation. Retroviral infection of Smurf2(WT) and Smurf2(T249E) decreased chondrocyte differentiation in control and Erk5-deficient cells (Fig. 5Ga,Gb,Gd-Gf,Gh), whereas Smurf2(T249A) increased the differentiation of control cells but not Erk5-deficient cells (Fig. 5Ga, Gc,Ge,Gg). Consistent with these results, but in contrast to the increase in activity following Smurf2(T249A) transfection, BRE-luc activity was lower in cells transfected with Smurf2(WT), with further decreases induced by Smurf2(T249E) transfection (Fig. 5H).

Collectively, these results suggest that the Mek5-Erk5 pathway regulates the stability of Smads by enhancing the ubiquitin E3 ligase activity of Smurf2 through direct phosphorylation at Thr[249] and by modulating the Smurf1-dependent proteasomal degradation of Smad1 through direct phosphorylation at Ser[206].

Smads directly activate Sox9 expression
Given that Erk5 deficiency induces *Sox9* mRNA transcription and Erk5 activates Smad proteasomal degradation by Smurf2, we tested whether Smads could activate Sox9 expression at the transcriptional level in mesenchymal cells. Introduction of Smad1 and Smad4 (Smad1/Smad4), Smad2 and Smad4 (Smad2/Smad4), and Smad3 and Smad4 (Smad3/Smad4) induced Sox9 protein (Fig. 6A) and mRNA expression (Fig. 6B). We computationally analyzed the 5′-flanking region of mouse *Sox9* and human *SOX9* and identified at least one putative bone morphogenic protein responsive element (BRE) and one putative Smad-binding element (SBE) in the 5′-flanking region, which were highly conserved between mouse and human *SOX9* (Fig. 6C). A reporter assay performed using primary mesenchymal cells revealed that introduction of Smad1/Smad4, Smad2/Smad4 and Smad3/Smad4 significantly activated *Sox9* promoter activity (Fig. 6D). Moreover, a chromatin IP assay verified that Smad1 recruitment to the *Sox9* promoter regions encompassing the BRE was enhanced in Erk5-deficient cells compared with control cells without a significant change in Smad2 and Smad3 recruitment (Fig. 6E). By contrast, recruitment of Smad2 and Smad3, but not Smad1, to the *Sox9* promoter regions encompassing the SBE was significantly increased in Erk5-deficient cells (Fig. 6F).
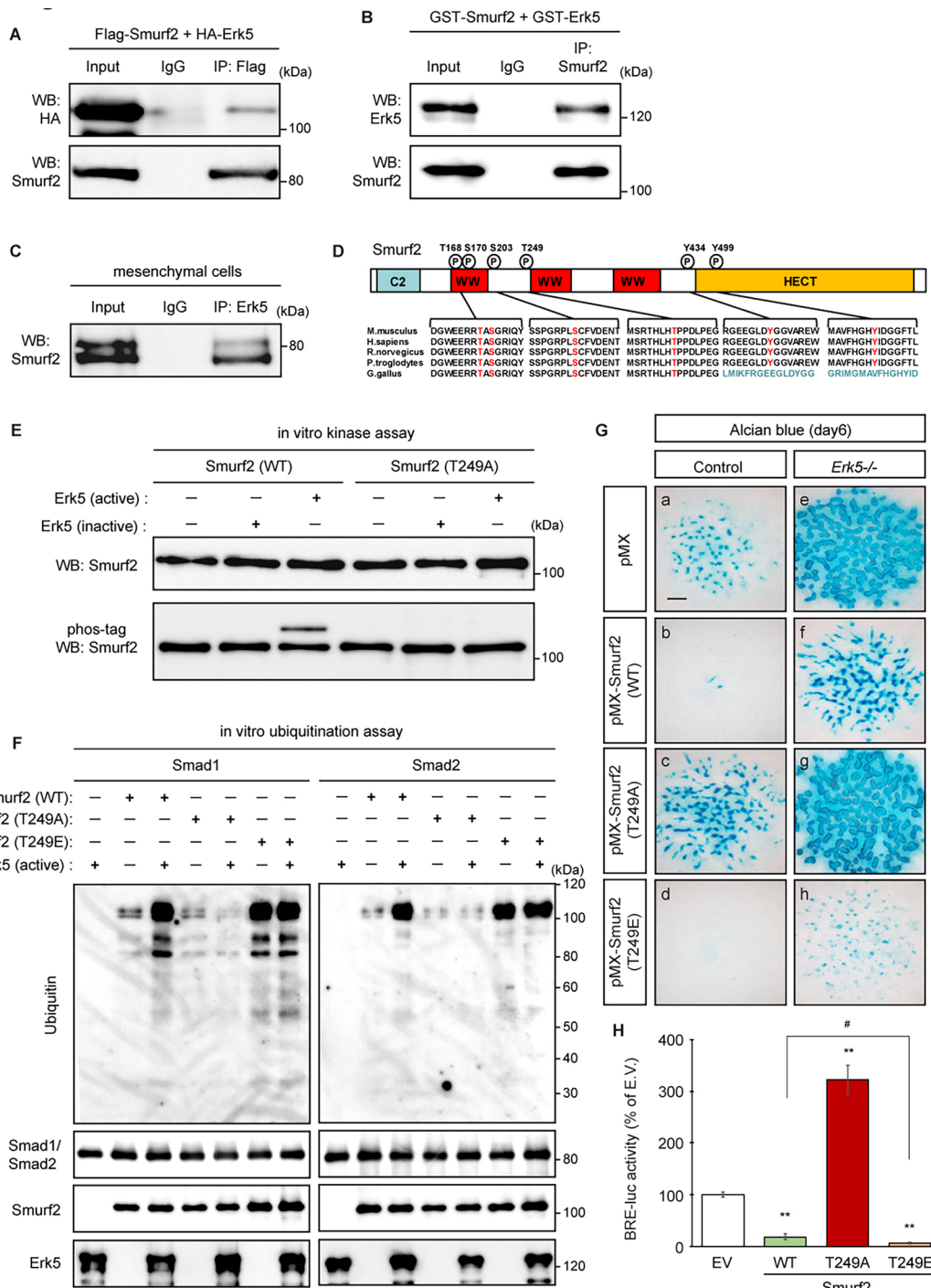
Fig. 5. Erk5 phosphorylates Smurf2 at Thr^{249} residue to accelerate Smad ubiquitylation. (A-C) IP assay in HEK293 cells (A), a cell-free system with recombinant proteins (B), and primary mesenchymal cells (C) (n=3). (D) Schematic of Smurf2 protein structure with the predicted phosphorylation sites and their conservation among vertebrates. (E) *In vitro* kinase assay. Recombinant Smuf2 proteins were incubated with active or inactive Erk5, followed by Phos-tag SDS-PAGE and subsequent immunoblotting (n=4). (F) *In vitro* ubiquitylation assay. Recombinant Smurf2 proteins and Smad proteins were incubated with active Erk5 in the presence of E1 and UbcH5c, followed by SDS-PAGE (n=4). (G) Primary mesenchymal cells from *Erk5$^{fl/fl}$* (control) and *Prx1-Cre;Erk5$^{fl/fl}$* (*Erk5$^{-/-}$*) embryos were retrovirally infected with Smurf2(WT), Smurf2(T249A) and Smurf2(T249E) vectors, followed by micromass culture and subsequent Alcian Blue staining at day 6 (n=5). (H) Primary mesenchymal cells were transiently co-transfected with BRE-luc vector and Smurf2(WT), Smurf2(T249A) or Smurf2(T249E) expression vectors, and subsequently luciferase activity was determined (n=5). **P<0.01 (significantly different from the value obtained in empty vector-transfected cells); #P<0.05 [significantly different from the value obtained in cells transfected with Smurf2(WT) vector] (one-way analysis of variance with Bonferroni post-hoc test). Error bars represent s.e.m. E.V., empty vector. Scale bar: 500 μm.

Erk5 regulates skeletogenesis through Sox9 *in vivo*

Our results suggest that Erk5 deficiency influences skeletogenesis and chondrogenesis through the activation of

Sox9 expression *in vitro* and *in vivo*. To investigate this genetically *in vivo*, we generated *Erk5$^{-/-}$* embryos lacking one allele at *Sox9* in mesenchymal cells. *Prx1-Cre;Erk5$^{fl/fl}$;Sox9$^{fl/+}$*
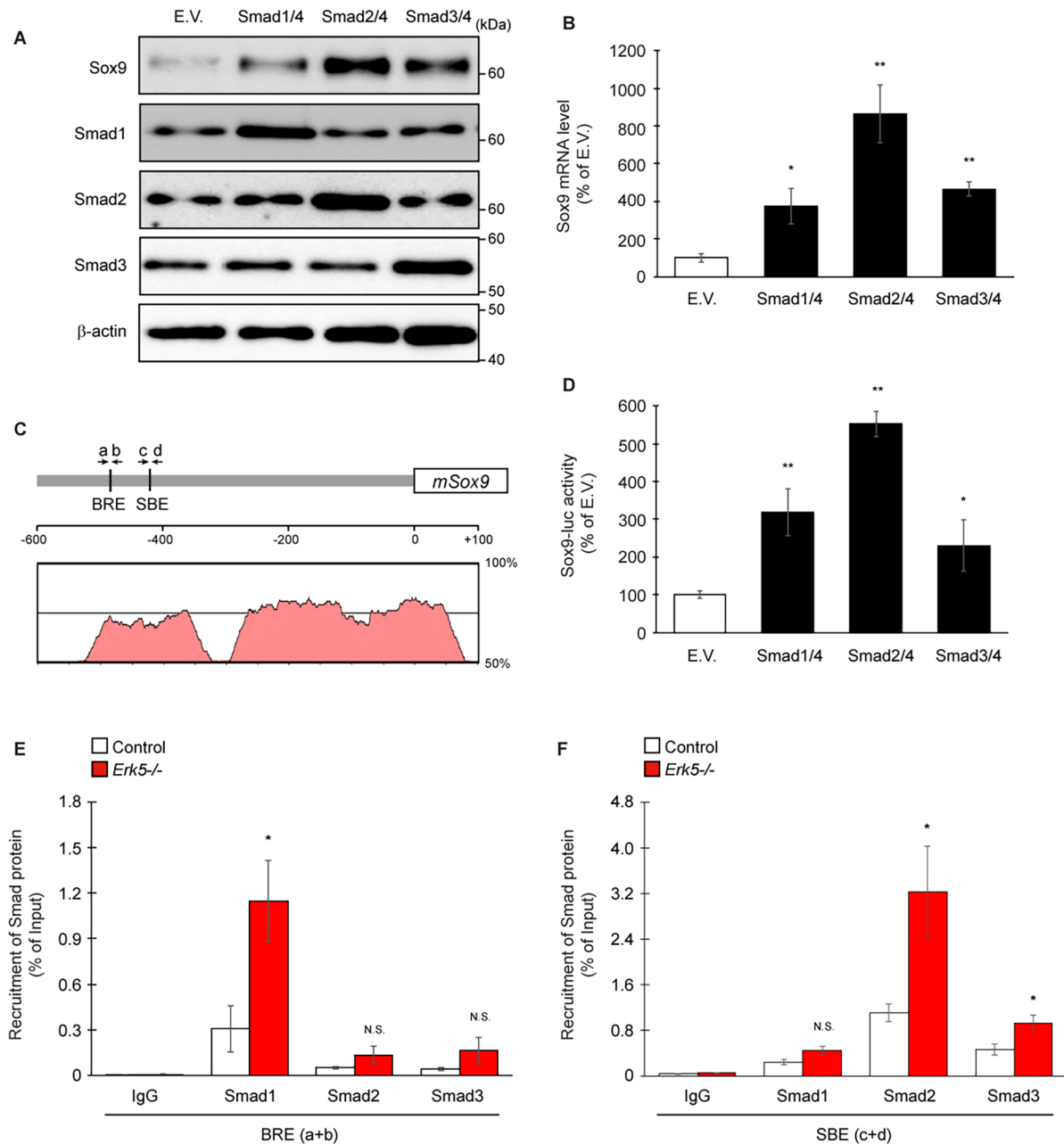
Fig. 6. Smad proteins directly activate Sox9 expression in mesenchymal cells. (A,B) Primary mesenchymal cells from wild-type embryos were transiently transfected with various Smad expression vectors, followed by determination of protein level (A) (n=3) and mRNA level (B) of Sox9 (n=5). (C) Schematic of the alignment of mouse *Sox9* promoter region with putative BRE and SBE in addition to primers (a-d) used for ChIP assays. Highly conserved regions between mouse and human were identified and colored orange in the graph below using VISTA tools (http://genome.lbl.gov/vista/index.shtml). (D) Primary mesenchymal cells from wild-type embryos were transiently co-transfected with Sox9-luc and various Smad expression vectors, followed by determination of luciferase activity (n=5). (E,F) Primary mesenchymal cells from *Erk5*$^{fl/fl}$ and (control) *Prx1-Cre;Erk5*$^{fl/fl}$ (*Erk5*$^{-/-}$) embryos were subjected to ChIP assay using anti-Smad1, anti-Smad2 and anti-Smad3 antibodies along with specific primers (a-d) to recognize *Sox9* promoter regions containing BRE (E) and SBE (F) (shown in the C) (n=6). *P<0.05, **P<0.01 [significantly different from the value obtained in cells transfected with empty vector (B,D)]; *P<0.05 [significantly different from the value obtained in control cells (E,F)]; two-tailed, unpaired Student's t-test. N.S., not significant. E.V., empty vector.

embryos and mice displayed partial normalization of abnormalities of the metatarsal and proximal phalanges at E18.5 (Fig. 7Am-Ap, Fig. S8A) and bone formation deformities in the feet at 3 weeks old (Fig. 7Aq-At). Moreover, *Sox9* heterodeficiency rescued the larger posterior fontanel identified in *Prx1-Cre;Erk5*$^{fl/fl}$ embryos (Fig. 7Ai-Al), whereas the width of the long bones in the forelimbs and hindlimbs was comparable between *Prx1-Cre;Erk5*$^{fl/fl}$ and *Prx1-Cre;Erk5*$^{fl/fl}$; *Sox9*$^{fl/+}$ embryos (Fig. 7Ae-Ah). Moreover, abnormalities of

differentiation and maturation in Erk5-deficient cells, defined as Alcian Blue-positive areas (Fig. 7Ba-Bd,C) and Alizarin Red intensity (Fig. 7Be-Bh,D), respectively, were rescued by *Sox9* heterodeficiency in mesenchymal cells *in vitro*. This result is correlated with the reduction of Sox9 protein levels in *Erk5*$^{-/-}$; *Sox9*$^{+/-}$ cells (Fig. S8B). Taken together, these results provide genetic evidence that Erk5 regulates skeletogenesis in part through its ability to inhibit Sox9 expression and function in mesenchymal cells.
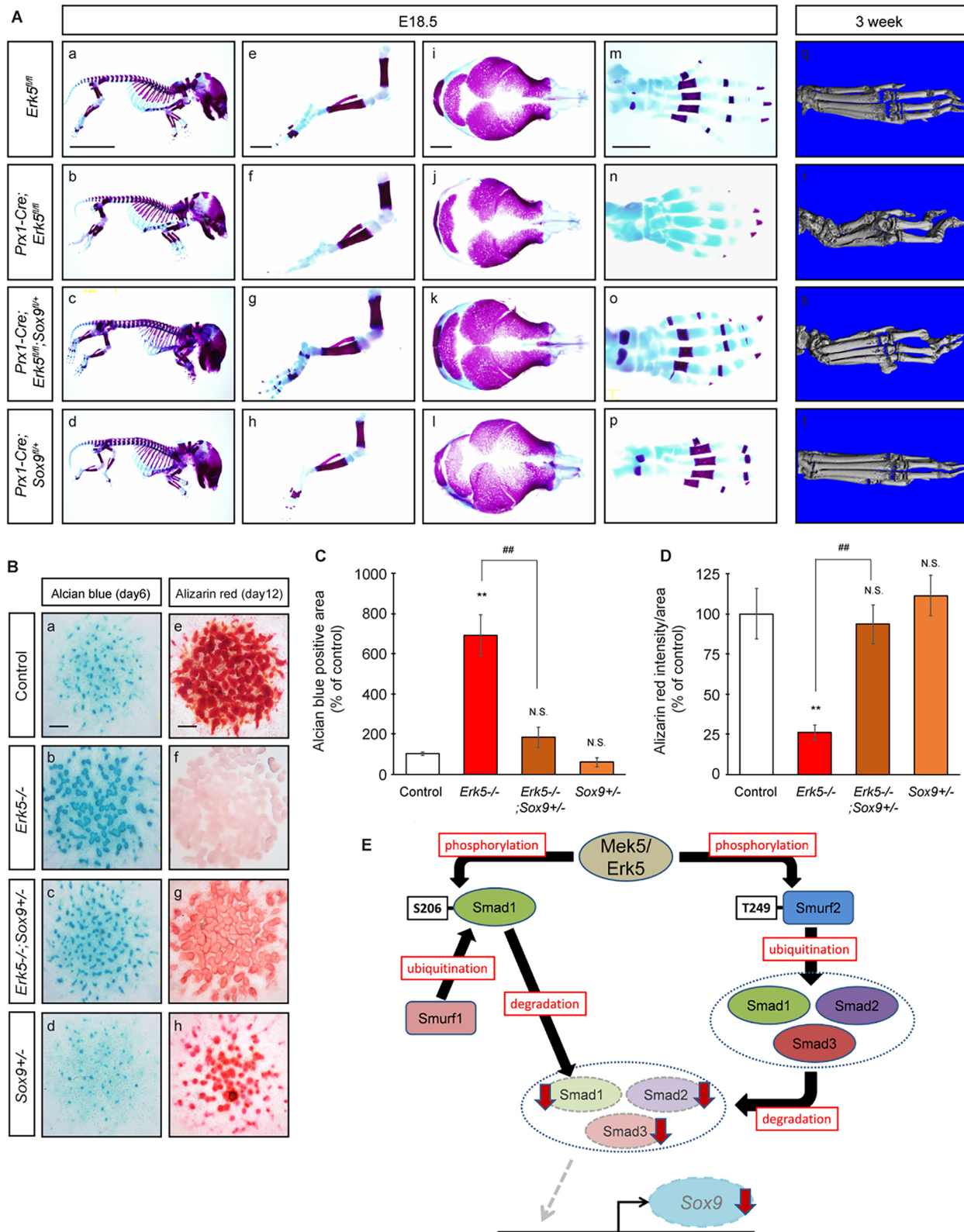
Fig. 7. Erk5 regulates skeletogenesis through Sox9. (A) The whole skeleton and parts of the skeleton of *Erk5^{fl/fl}*, *Prx1-Cre;Erk5^{fl/fl}*, *Prx1-Cre;Erk5^{fl/fl};Sox9^{fl/+}* and *Prx1-Cre;Sox9^{fl/+}* embryos at E18.5 (Aa-Ap) and µCT 3D images of the foot of mutant mice at 3 weeks (Aq-At). Embryos were double stained with Alizarin Red and Alcian Blue. Representative images of skeletal preparations derived from more than three mice from different litters are shown. (B-D) Micromass culture of dissociated mesenchymal cells of *Erk5^{fl/fl}* (control), *Prx1-Cre;Erk5^{fl/fl}* (*Erk5^{−/−}*), *Prx1-Cre;Erk5^{fl/fl};Sox9^{fl/+}* (*Erk5^{−/−};Sox9^{+/−}*) and *Prx1-Cre;Sox9^{fl/+}* (*Sox9^{+/−}*) embryos at E12.5 was performed, followed by determination of Alcian Blue staining at day 6 (Ba-Bd,C) and Alizarin Red staining at day 12 (Be-Bh,D) (*n*=5). (E) Schematic model of the findings of this study. Erk5 phosphorylates Smad1 and Smurf2. These functions enhance ubiquitylation of Smad proteins to inhibit Sox9 expression. **$P<0.01$ (significantly different from the value obtained in control cells); ##$P<0.01$ (significantly different from the value obtained in Erk5-deficent cells); one-way analysis of variance with Bonferroni post-hoc test. N.S., not significant. Error bars represent s.e.m. Scale bars: 10 mm (Aa-Ad); 1 mm (Ae-Ap); 500 µm (B).

DISCUSSION

Previous *in vitro* studies revealed the role of Erk5 as a negative regulator of chondrocyte differentiation (Bobick et al., 2010; Wang et al., 2016). However, *Erk5* knockout in mice is embryonically lethal at E9.5-10.5 (Regan et al., 2002; Yan et al., 2003); therefore, the *in vivo* physiological role of Erk5 in skeletal development has remained largely unclear. The present findings reveal that Erk5 deficiency in mesenchymal cells leads to abnormal skeletogenesis *in vivo*. Moreover, several lines of evidence indicate that Mek5-Erk5 signaling controls chondrogenic differentiation by modulating the protein stability of Smads (Smad1, Smad2 and Smad3), which activate Sox9 expression at the transcriptional level through at least two pathways. First, Erk5 directly phosphorylates Smad1 at Ser[206] to trigger its proteasomal degradation in a Smurf1-dependent manner. Second, Erk5 directly phosphorylates Smurf2 at Thr[249] to activate its ubiquitin E3 ligase ability to degrade Smad proteins (Smad1, Smad2 and Smad3). Although we should emphasize that this cascade is not activated in all skeletal elements and we have not linked their mechanistic *in vitro* studies to the phenotypic alternations by examining the relevant players *in vivo*, to our knowledge, this is the first direct demonstration of the role for the Mek5-Erk5 pathway in skeletogenesis *in vivo* in modulating chondrogenic differentiation through the Smurf-Smad-Sox9 cascade (Fig. 7E).

The possibility should be mentioned that Erk5 controls chondrogenic differentiation through its expression in perichondrium cells, which are targeted by *Prx1-Cre* and *Col2a1-Cre* (Ono et al., 2014). However, *Osx-Cre;Erk5^{fl/fl}* embryos did not exhibit any abnormalities in skeletal phenotypes (Fig. S4) despite the activity of *Osx-Cre* in the perichondrium (Rodda and McMahon, 2006). Thus, although further studies are needed, these results suggest that Erk5 does not directly control growth plate cartilage development or endochondral ossification through its expression in the perichondrium.

It should also be noted that the data from two different phenotypes of *Prx1-Cre;Erk5^{fl/fl}* embryos (wider bones and mineralization defect/delay) should be interpreted as two different developmental processes. The mineralization area was markedly decreased in the metatarsals, but not in tibia and femur, in *Prx1-Cre; Erk5^{fl/fl}* embryos at E16.5 and E18.5, suggesting the mineralization defect or delay is specific to the development of distal skeletal elements, although it cannot be ruled out that a transient delay in hypertrophic differentiation/mineralization may occur in the proximal skeletal elements at an earlier developmental time point. Many genetic diseases with brachydactylies, which are inheritable conditions typified by short fingers and toes, has been reported to be related to malfunction of BMP/TGFβ and hedgehog signaling that affect distal chondrogenic events with delayed mineralization of digit cartilage elements (Gao et al., 2001, 2009; Lehmann et al., 2003). To identify the processes or molecular signals involved in the distal preference of mineralization defects or delays in *Prx1-Cre;Erk5^{fl/fl}* embryos, we should test whether the Mek5-Erk5 pathway is a downstream or upstream effector of BMP/TGFβ or hedgehog signaling in mesenchymal cells. However, the possibility of a more general effect of Erk5 on fibroblast differentiation or proliferation, with chondrogenesis being a downstream consequence, should be considered, although the fact that Erk5-deficient CD45−CD29+Sca1+CD105+ mesenchymal stem cells exhibited higher chondrogenic differentiation capacity could indicate a direct role of Erk5 in chondrogenic differentiation through its expression in mesenchymal progenitor cells.

We also demonstrated that Thr[249] is required for the E3 ubiquitin ligase activity of Smurf2. Replacing this residue with alanine (Smurf2-T249A) attenuated the ability of Smurf2 to degrade Smad proteins, whereas replacement with glutamate (Smurf2-T249E) led to greater degradation (Fig. 5, Fig. S7). Although Akt phosphorylates Smurf2 at unknown residues to induce Smurf2 degradation (Choi et al., 2014), our study clearly identified the particular phosphorylation site of Smurf2 (Thr[249]) and its target proteins (Smads) for regulating cellular function (chondrogenic differentiation) and uncovered the E3 ubiquitin ligase activity. Among the large number of target proteins of Smurf2 (Lin et al., 2000; Zhang et al., 2001; David et al., 2013), we focused on Smad1, Smad2 and Smad3, because Erk5 deficiency led to their upregulation at the protein but not mRNA level (Fig. 3). Smurf2 is known to directly and indirectly induce the ubiquitylation and degradation of multiple target proteins implicated in chondrogenesis, including the type I receptor of TGFβ, which is upstream of Smad2 and Smad3, as well as glycogen synthase kinase 3β and β-catenin (Kavsak et al., 2000; Han et al., 2006; Wu et al., 2009). Erk5 positively affects TGFβ-dependent Smad3 transcriptional activity via acetylation (Kim et al., 2013). We therefore cannot exclude the possibility that another pathway could also contribute to the regulation of Erk5-dependent skeletogenesis.

Moreover, for the first time, we revealed that Smads (Smad1/Smad4, Smad2/Smad4 and Smad3/Smad4) directly activated Sox9 expression at the transcriptional level in mesenchymal cells. As it has been demonstrated that Smad2 and Smad3 physically interact with Sox9, leading to the enhancement of its transcriptional activity (Furumatsu et al., 2005; Song et al., 2009), it is possible that Smads could regulate chondrogenic differentiation following Erk5-dependent induction by binding to Sox9 to enhance its transcriptional activity. This would induce the expression of chondrocyte-specific genes, including *Col2a1* and *Acan*, carrying Sox9-binding sites in their promoters (Lefrebvre and de Crombrugghe, 1998; Akiyama et al., 2002), in addition to directly inducing *Sox9* transcription in mesenchymal cells. Alternatively, Erk5 might control Sox9 levels through Smad-independent mechanisms, for example, through the control of *Sox9* RNA stability.

In conclusion, the Mek5-Erk5 pathway plays a crucial role in skeletogenesis *in vivo* by modulating the protein stability of Smads (Smad1, Smad2 and Smad3) via Smurfs (Smurf1 and Smurf2) through Smad expression in mesenchymal cells (Fig. 7E). Our findings improve our understanding of the molecular mechanisms underlying skeletal development, and they may lead to the development of novel drugs targeting cartilage diseases associated with abnormal chondrocyte differentiation and maturation in humans. Indeed, the Smurf-Smad cascade is associated with various human diseases, including cancer and aging (Fukuchi et al., 2002; Zhang and Cohen, 2004; Jin et al., 2009). Therefore, components of the Mek5-Erk5-Smurf-Smad-Sox9 cascade could represent novel targets for drug development to treat various human diseases.

MATERIALS AND METHODS
Mice

Erk5^{fl/fl} (Newbern et al., 2011) and *Sox9^{fl/fl}* (Akiyama et al., 2002) mice were crossed with either *Prx1-Cre* (Logan et al., 2002), *Col2a1-Cre* (Terpstra et al., 2003) or *Osx-Cre* (Takarada et al., 2016). These mutant mice were backcrossed for more than five generations with C57BL/6J. Mice were bred under standard animal housing conditions at 23±1°C with humidity of 55% and a 12 h light/dark cycle, with free access to food and water. Genotyping

was performed by PCR using tail genomic DNA. The study protocol meets the guidelines of the Japanese Pharmacological Society and was approved by the Committee for Ethical Use of Experimental Animals at Kanazawa University, Kanazawa, Japan. The numbers of animals used per experiment are stated in the figure legends.

Skeletal preparation, histological analysis, *in situ* hybridization analysis and immunohistochemical analysis

Embryos were eviscerated and the skins were removed, then embryos were fixed in 95% ethanol overnight. Embryos were then immersed in Alcian Blue solution overnight, and were transferred in a solution of 2% KOH overnight, followed by staining in Alizarin Red solution overnight. Finally, the skeletons were cleaned with 1% KOH/20% glycerol for 1 week and then stored in 50% ethanol/50% glycerol (Takahata et al., 2012). For micro computed tomography (μCT) 3D images of the foot were obtained using a VivaCT 40 mCT system (Scanco Medical) as described previously (Kajimura et al., 2011).

Mouse tibia, femurs and feet were fixed with 10% formalin neutral buffer solution overnight, embedded in paraffin, and then sectioned at a thickness of 5 μm. Sections were stained with H&E, Safranin O and von Kossa.

In situ hybridization was performed as previously described (Wang et al., 2005). In brief, the metatarsals were dissected in a cryostat to yield frozen sections with a thickness of 10 μm. Sections mounted on glass slides were fixed with 4% paraformaldehyde and successively treated with 0.2 M HCl for 10 min and 10 μg/ml proteinase K for 5 min. Sections were then subjected to acetylation in 0.1 M triethanolamine with 0.25% acetic anhydride for 10 min. After prehybridization, sections were covered with digoxigenin-labeled cRNA probes at 65°C for 16 h. Sections were then washed and treated with 4 μg/ml RNase A for 30 min. Sections were further incubated with anti-digoxigenin-ALP Fab fragments for 16 h. After washing, sections were treated with nitro blue tetrazolium chloride/5-bromo-4-chloro-3-indolyl phosphate for different periods. Plasmid vectors for generating cRNA probes were kindly provided by Dr Nishimura (Osaka University, Osaka, Japan) and Dr Ducy (Columbia University, NY, USA).

For immunohistochemistry, 5-μm-thick sections were deparaffinized in xylene and rehydrated in ethanol. Antigen retrieval was performed in citrate buffer (pH 6.0). After treatment with blocking buffer (PBS containing 0.5% Triton X-100 and 5% normal goat serum) for 1 h, the sections were incubated with anti-Sox9 antibody (EMD Millipore) in blocking buffer for 24 h. The sections were further incubated with anti-rabbit IgG (Alexa Fluor 488) in blocking buffer for 2 h.

For whole-mount immunohistochemistry, limb buds were fixed with methanol:dimethyl sulfoxide (4:1) overnight, and were washed three times with 1% Triton X-100/PBS. After treatment with blocking buffer (PBS containing 1% Triton X-100 and 5% normal goat serum) for 1 h, limb buds were incubated with anti-Sox9 antibody in blocking buffer for 24 h, followed by incubation with anti-rabbit IgG (Alexa Fluor 488) in blocking buffer for 48 h.

Generation of retroviral vectors and infection

To generate the mutant Smurf2 constructs [pMX-Smurf2(T249A) and pMX-Smurf2(T249E)], site-directed mutagenesis was performed using the PrimeSTAR Max Mutagenesis Basal Kit (Takara Bio) with specific primers (Table S1). pMX-Erk5(WT) and pMX-Erk5(DN) vectors were generated by subcloning into pMX vector from pcDNA3-Erk5(WT) and pcDNA3-Erk5AEF vectors, respectively, which were generously provided by Dr Jiing-Dwan Lee (Scripps Research Institute, CA, USA). These vectors were then transfected into PLAT-E cells using the calcium carbonate method. Virus supernatant was collected 48 h after transfection and cells were then infected with this viral supernatant for 8 h in the presence of 4 μg/ml polybrene.

Micromass culture system

Whole limb bud mesenchymal cells from E12.5 were treated with 0.1% collagenase and 0.1% dispase for 1.5 h at 37°C, and subsequently re-suspended in DMEM/F12 medium containing 10% fetal bovine serum (FBS) at 1.5×10^7 cells/ml. Droplets were carefully placed in each well of a

4-well plate. Cells were allowed to adhere at 37°C for 1.5 h, followed by the addition of chondrogenic medium (DMEM/F12 medium containing 10% FBS and 50 μg/ml ascorbic acid). Medium was changed every 2 days, and Alcian Blue and Alizarin Red staining was performed on day 6 and day 12, respectively.

Limb bud mesenchymal cells from E12.5 were digested and re-suspended in PBS containing 2% FBS, followed by incubation for 30 min at 4°C with FITC anti-CD45 antibody (1:40, 30-F11, BD Pharmingen), APC anti-CD105 antibody (1:40, MJ7/18, eBioscience), PE anti-CD29 antibody (1:40, HMβ1-1, BioLegend), PE-Cy7 anti-Ly6A/E antibody (1:40, D7, BD Pharmingen) and DAPI for dead cell exclusion. Immunostained cells were analyzed on FACS AriaII cell sorter (BD Biosciences), and subsequently FITC-negative and APC-, PE-, PE-Cy7-positive cells were sorted, followed by re-suspension in DMEM/F12 medium containing 10% FBS at 1.5×10^7 cells/ml. Cells were allowed to adhere at 37°C for 1.5 h, followed by the addition of chondrogenic medium (DMEM/F12 medium containing 10% FBS, 50 μg/ml ascorbic acid, 0.1 M dexamethasone, 1 mM sodium pyruvate and 20 ng/ml TGFβ).

Real-time quantitative PCR

Total RNA was extracted from cells, followed by the synthesis of cDNA using reverse transcriptase and oligo-dT primer. The cDNA samples were then used as templates for real-time PCR analysis, which was performed on an MX3005P qPCR System (Agilent Technologies) using specific primers for each gene (Table S2). The levels of the genes examined were normalized using *Actb* as an internal control for each sample.

Immunoblotting analysis

Cells were solubilized in lysis buffer containing 1% Nonidet P-40. Samples were then subjected to sodium dodecyl sulfate-polyacrylamide gel electrophoresis (SDS-PAGE), followed by transfer to polyvinylidine difluoride membranes (PVDF) and subsequent immunoblotting. The primary antibodies used were: anti-Runx2 (1:1000, #8486), anti-Erk5 (1:1000, #3372), anti-Smad1 (1:1000, #9743), anti-Smad2 (1:1000, #5339), anti-Smad3 (1:1000, #9523), anti-phospho-Smad1/5/8 (1:1000, #13820), anti-phospho-Smad2/3 (1:1000, #8828) and anti-phospho-Erk5 (1:1000, #3371) (all from Cell Signaling Technologies); anti-β-actin (1:2000, C4), anti-Smad5 (1:1000, D-20), anti-Smad8 (1:1000, R-64) and anti-Smurf2 (1:1000, H-50) (all from Santa Cruz Biotechnology); anti-Sox9 (1:2000, #AB5535, EMD Millipore); and anti-Osx (1:1000, #ab94744, Abcam).

Luciferase assay

Plasmids BRE-luc (#45126) (artificial sequences) and SBE4-luc (#16495) (conserved sequences between human and mouse) were obtained from Addgene, and plasmids Runx2-luc and 6xOSE2-luc were kindly provided by Dr Ducy (Columbia University, NY, USA). Plasmid 4x48-luc was generously provided by Dr Crombrugghe (University of Texas, M.D. Anderson Cancer Center, TX, USA). For the luciferase assay, cells were transfected with reporter vectors using the lipofection method as previously described (Hinoi et al., 2012), followed by the preparation of cell lysates and subsequent determination of luciferase activity using specific substrates in a luminometer (ATTO). Transfection efficiency was normalized by determining *lacZ* activity by using an ONPG assay.

ChIP assay

ChIP experiments were performed following the protocol provided with the ChIP assay kit (EMD Millipore). Cells were treated with formaldehyde to induce cross-linking and were subsequently subjected to sonication in lysis buffer. IP was performed with the anti-Smad1, anti-Smad2 or anti-Smad3 antibodies used at 1:50 dilution, followed by PCR with specific primers (Table S3).

Preparation of recombinant proteins

Recombinant GST-tagged human Smad1, Smad2 and Smad3 proteins and recombinant full-length Erk5 active were purchased from Sigma-Aldrich, and recombinant Erk5 inactive was obtained from Carna Biosciences. The mutant *Smad1* constructs were generated with site-directed mutagenesis

using the PrimeSTAR Max Mutagenesis Basal Kit with specific primers (Table S4). Human *SMAD1* (WT and mutants), and *SMURF2* (WT and mutants) cDNA were inserted into pCold II vector (Takara Bio) with N-terminal GST-tag. GST-tagged vectors were expressed in *Escherichia coli* strain BL21 cultured with 50 µM isopropyl-β-D-thiogalactopyranoside at 15°C for 24 h. The bacterial cells were centrifuged at 3000 *g* and the supernatant removed. The bacterial pellets were subjected to freeze/thaw treatment three times and then incubated in lysis buffer (50 mM Tris-HCl, 500 mM NaCl, 10% glycerol, 1% Triton X-100, pH 8.0 at 4°C) containing 1 mg/ml lysozyme for 30 min, followed by sonication. GST-tagged proteins in the supernatant were purified by a column packed with Glutathione Sepharose 4 Fast Flow (GE Healthcare). The GST-tagged proteins were eluted with the buffer (100 mM Tris-HCl, 20 mM glutathione, pH 8.0 at 4°C). The eluted proteins were dialyzed for 24 h at 4°C against repeated changes of dialysis buffer (10 mM Tris-HCl, pH 7.5).

IP assay
Plasmids Flag-Smurf2 (#11746, deposited by Jeff Wrana) and HA-Erk5 (#31817, deposited by Astar Winoto) were obtained from Addgene. HEK293 cells were transiently transfected with expression vectors using the calcium phosphate transfection method, and cells were then solubilized in lysis buffer containing 1% Nonidet P-40, followed by incubation with an antibody for 1 h at 4°C and subsequent IP with protein G-Sepharose. Recombinant proteins were incubated with an antibody in binding buffer containing 0.5% Nonidet P-40 for 1 h at 4°C and subsequent IP with protein G-Sepharose. Immunoprecipitates were washed three times with lysis buffer or binding buffer and boiled in SDS sample buffer. Samples were then separated by SDS-PAGE, followed by transfer to PVDF membranes and subsequent immunoblotting, as previously described (Nakamura et al., 2013).

In vitro kinase assay
Recombinant Erk5 active or recombinant Erk5 inactive (0.3 µM) were incubated with GST-Smad1(WT and mutants), GST-Smad2(WT), GST-Smad3(WT) or GST-Smurf2(WT and mutants) (1 µM) and 0.5 mM ATP in 30 µl kinase buffer (2.5 mM MOPS, pH 7.2, 2.5 mM $MgCl_2$, 1.25 mM glycerol 2-phosphate, 0.25 mM DTT, 0.05% bovine serum albumin) for 30 min at 30°C. The reaction was stopped by adding SDS sample buffer. Phosphorylated proteins were analyzed by Phos-tag PAGE. For Phos-tag immunoblotting, 0.05 mM Phos-tag (Wako) and 0.1 mM $MnCl_2$ were added to conventional SDS polyacrylamide gels according to the manufacturer's protocol.

In vitro ubiquitylation assay
In vitro ubiquitylation assay was performed with the E2-Ubiquitin Conjugation Kit (Abcam) following the protocol recommended by the manufacturer. GST-Smad1, GST-Smad2 or GST-Smad3 (1 µM) were incubated with GST-Smurf2(WT and mutants) (0.1 µM) and GST-Erk5 active (0.05 µM) in 1×Ubiquitylation Buffer [0.1 µM E1, 0.5 µM UbcH5c (E2), 5 mM Mg-ATP, 1 mM DTT, 2.5 µM biotinylated ubiquitin] for 1 h at 37°C. The reaction was stopped by adding 2×Non-reducing gel loading buffer. Ubiquitylated proteins were analyzed by SDS-PAGE and horseradish peroxidase-conjugated streptavidin detection system.

Immunocytochemical analysis
For immunocytochemical analysis, cells were plated on a chamber slide coated with poly-L-lysine. Cultured cells were fixed with 4% paraformaldehyde in PBS, followed by washing and subsequent treatment with normal goat serum in PBS containing 0.1% Triton X-100. Cells were then incubated with a primary antibody diluted in PBS containing normal goat serum and 0.3% Triton X-100. Finally, cells were reacted with the corresponding secondary antibody and chamber slides were mounted using FluorSave (EMD Millipore).

Data analysis
All results are expressed as the mean±s.e.m., and statistical significance was determined using two-tailed, unpaired Student's *t*-test or one-way analysis of variance with Bonferroni post-hoc test.

References
Akiyama, H., Chaboissier, M. C., Martin, J. F., Schedl, A. and de Crombrugghe, B. (2002). The transcription factor Sox9 has essential roles in successive steps of the chondrocyte differentiation pathway and is required for expression of Sox5 and Sox6. *Genes Dev.* **16**, 2813-2828.

Bentires-Alj, M., Kontaridis, M. I. and Neel, B. G. (2006). Stops along the RAS pathway in human genetic disease. *Nat. Med.* **12**, 283-285.

Bobick, B. E., Matsche, A. I., Chen, F. H. and Tuan, R. S. (2010). The ERK5 and ERK1/2 signaling pathways play opposing regulatory roles during chondrogenesis of adult human bone marrow-derived multipotent progenitor cells. *J. Cell. Physiol.* **224**, 178-186.

Buschbeck, M. and Ullrich, A. (2005). The unique C-terminal tail of the mitogen-activated protein kinase ERK5 regulates its activation and nuclear shuttling. *J. Biol. Chem.* **280**, 2659-2667.

Chang, L. and Karin, M. (2001). Mammalian MAP kinase signalling cascades. *Nature* **410**, 37-40.

Chen, Z., Yue, S. X., Zhou, G., Greenfield, E. M. and Murakami, S. (2015). ERK1 and ERK2 regulate chondrocyte terminal differentiation during endochondral bone formation. *J. Bone Miner. Res.* **30**, 765-774.

Choi, Y. H., Kim, Y.-J., Jeong, H. M., Jin, Y.-H., Yeo, C.-Y. and Lee, K. Y. (2014). Akt enhances Runx2 protein stability by regulating Smurf2 function during osteoblast differentiation. *FEBS J.* **281**, 3656-3666.

Cserjesi, P., Lilly, B., Bryson, L., Wang, Y., Sassoon, D. A. and Olson, E. N. (1992). MHox: a mesodermally restricted homeodomain protein that binds an essential site in the muscle creatine kinase enhancer. *Development* **115**, 1087-1101.

David, D., Nair, S. A. and Pillai, M. R. (2013). Smurf E3 ubiquitin ligases at the cross roads of oncogenesis and tumor suppression. *Biochim. Biophys. Acta* **1835**, 119-128.

English, J. M., Vanderbilt, C. A., Xu, S., Marcus, S. and Cobb, M. H. (1995). Isolation of MEK5 and differential expression of alternatively spliced forms. *J. Biol. Chem.* **270**, 28897-28902.

Fukuchi, M., Fukai, Y., Masuda, N., Miyazaki, T., Nakajima, M., Sohda, M., Manda, R., Tsukada, K., Kato, H. and Kuwano, H. (2002). High-level expression of the Smad ubiquitin ligase Smurf2 correlates with poor prognosis in patients with esophageal squamous cell carcinoma. *Cancer Res.* **62**, 7162-7165.

Furumatsu, T., Tsuda, M., Taniguchi, N., Tajima, Y. and Asahara, H. (2005). Smad3 induces chondrogenesis through the activation of SOX9 via CREB-binding protein/p300 recruitment. *J. Biol. Chem.* **280**, 8343-8350.

Gao, B., Guo, J., She, C., Shu, A., Yang, M., Tan, Z., Yang, X., Guo, S., Feng, G. and He, L. (2001). Mutations in IHH, encoding Indian hedgehog, cause brachydactyly type A-1. *Nat. Genet.* **28**, 386-388.

Gao, B., Hu, J., Stricker, S., Cheung, M., Ma, G., Law, K. F., Witte, F., Briscoe, J., Mundlos, S., He, L. et al. (2009). A mutation in Ihh that causes digit abnormalities alters its signalling capacity and range. *Nature* **458**, 1196-1200.

Han, G., Li, A. G., Liang, Y.-Y., Owens, P., He, W., Lu, S., Yoshimatsu, Y., Wang, D., Ten Dijke, P., Lin, X. et al. (2006). Smad7-induced beta-catenin degradation alters epidermal appendage development. *Dev. Cell* **11**, 301-312.

Hayashi, M., Kim, S.-W., Imanaka-Yoshida, K., Yoshida, T., Abel, E. D., Eliceiri, B., Yang, Y., Ulevitch, R. J. and Lee, J.-D. (2004). Targeted deletion of BMK1/ERK5 in adult mice perturbs vascular integrity and leads to endothelial failure. *J. Clin. Invest.* **113**, 1138-1148.

Hinoi, E., Ochi, H., Takarada, T., Nakatani, E., Iezaki, T., Nakajima, H., Fujita, H., Takahata, Y., Hidano, S., Kobayashi, T. et al. (2012). Positive regulation of

osteoclastic differentiation by growth differentiation factor 15 upregulated in osteocytic cells under hypoxia. *J. Bone Miner. Res.* **27**, 938-949.

Jin, C., Yang, Y.-A., Anver, M. R., Morris, N., Wang, X. and Zhang, Y. E. (2009). Smad ubiquitination regulatory factor 2 promotes metastasis of breast cancer cells by enhancing migration and invasiveness. *Cancer Res.* **69**, 735-740.

Johnson, R. L. and Tabin, C. J. (1997). Molecular models for vertebrate limb development. *Cell* **90**, 979-990.

Kajimura, D., Hinoi, E., Ferron, M., Kode, A., Riley, K. J., Zhou, B., Guo, X. E. and Karsenty, G. (2011). Genetic determination of the cellular basis of the sympathetic regulation of bone mass accrual. *J. Exp. Med.* **208**, 841-851.

Karsenty, G., Kronenberg, H. M. and Settembre, C. (2009). Genetic control of bone formation. *Annu. Rev. Cell Dev. Biol.* **25**, 629-648.

Kavsak, P., Rasmussen, R. K., Causing, C. G., Bonni, S., Zhu, H., Thomsen, G. H. and Wrana, J. L. (2000). Smad7 binds to Smurf2 to form an E3 ubiquitin ligase that targets the TGF beta receptor for degradation. *Mol. Cell* **6**, 1365-1375.

Kim, S., Lim, J. H. and Woo, C.-H. (2013). ERK5 inhibition ameliorates pulmonary fibrosis via regulating Smad3 acetylation. *Am. J. Pathol.* **183**, 1758-1768.

Kronenberg, H. M. (2003). Developmental regulation of the growth plate. *Nature* **423**, 332-336.

Lefebvre, V. and de Crombrugghe, B. (1998). Toward understanding SOX9 function in chondrocyte differentiation. *Matrix Biol.* **16**, 529-540.

Lehmann, K., Seemann, P., Stricker, S., Sammar, M., Meyer, B., Suring, K., Majewski, F., Tinschert, S., Grzeschik, K.-H., Muller, D. et al. (2003). Mutations in bone morphogenetic protein receptor 1B cause brachydactyly type A2. *Proc. Natl. Acad. Sci. USA* **100**, 12277-12282.

Li, T., Pan, Y.-W., Wang, W., Abel, G., Zou, J., Xu, L., Storm, D. R. and Xia, Z. (2013). Targeted deletion of the ERK5 MAP kinase impairs neuronal differentiation, migration, and survival during adult neurogenesis in the olfactory bulb. *PLoS ONE* **8**, e61948.

Lin, X., Liang, M. and Feng, X.-H. (2000). Smurf2 is a ubiquitin E3 ligase mediating proteasome-dependent degradation of Smad2 in transforming growth factor-beta signaling. *J. Biol. Chem.* **275**, 36818-36822.

Logan, M., Martin, J. F., Nagy, A., Lobe, C., Olson, E. N. and Tabin, C. J. (2002). Expression of Cre Recombinase in the developing mouse limb bud driven by a Prxl enhancer. *Genesis* **33**, 77-80.

Long, F. (2012). Building strong bones: molecular regulation of the osteoblast lineage. *Nat. Rev. Mol. Cell Biol.* **13**, 27-38.

Long, F. and Ornitz, D. M. (2013). Development of the endochondral skeleton. *Cold Spring Harb. Perspect. Biol.* **5**, a008334.

Maes, C. (2013). Role and regulation of vascularization processes in endochondral bones. *Calcif. Tissue Int.* **92**, 307-323.

Matsushita, T., Chan, Y. Y., Kawanami, A., Balmes, G., Landreth, G. E. and Murakami, S. (2009). Extracellular signal-regulated kinase 1 (ERK1) and ERK2 play essential roles in osteoblast differentiation and in supporting osteoclastogenesis. *Mol. Cell. Biol.* **29**, 5843-5857.

Nakamura, Y., Hinoi, E., Iezaki, T., Takada, S., Hashizume, S., Takahata, Y., Tsuruta, E., Takahashi, S. and Yoneda, Y. (2013). Repression of adipogenesis through promotion of Wnt/beta-catenin signaling by TIS7 up-regulated in adipocytes under hypoxia. *Biochim. Biophys. Acta* **1832**, 1117-1128.

Newbern, J. M., Li, X., Shoemaker, S. E., Zhou, J., Zhong, J., Wu, Y., Bonder, D., Hollenback, S., Coppola, G., Geschwind, D. H. et al. (2011). Specific functions for ERK/MAPK signaling during PNS development. *Neuron* **69**, 91-105.

Nishimoto, S. and Nishida, E. (2006). MAPK signalling: ERK5 versus ERK1/2. *EMBO Rep.* **7**, 782-786.

Nithianandarajah-Jones, G. N., Wilm, B., Goldring, C. E. P., Müller, J. and Cross, M. J. (2014). The role of ERK5 in endothelial cell function. *Biochem. Soc. Trans.* **42**, 1584-1589.

Ono, N., Ono, W., Nagasawa, T. and Kronenberg, H. M. (2014). A subset of chondrogenic cells provides early mesenchymal progenitors in growing bones. *Nat. Cell Biol.* **16**, 1157-1167.

Raman, M., Chen, W. and Cobb, M. H. (2007). Differential regulation and properties of MAPKs. *Oncogene* **26**, 3100-3112.

Rauen, K. A. (2013). The RASopathies. *Annu. Rev. Genomics Hum. Genet.* **14**, 355-369.

Regan, C. P., Li, W., Boucher, D. M., Spatz, S., Su, M. S. and Kuida, K. (2002). Erk5 null mice display multiple extraembryonic vascular and embryonic cardiovascular defects. *Proc. Natl. Acad. Sci. USA* **99**, 9248-9253.

Robinson, M. J. and Cobb, M. H. (1997). Mitogen-activated protein kinase pathways. *Curr. Opin. Cell Biol.* **9**, 180-186.

Rodda, S. J. and McMahon, A. P. (2006). Distinct roles for Hedgehog and canonical Wnt signaling in specification, differentiation and maintenance of osteoblast progenitors. *Development* **133**, 3231-3244.

Rodriguez-Viciana, P., Tetsu, O., Tidyman, W. E., Estep, A. L., Conger, B. A., Cruz, M. S., McCormick, F. and Rauen, K. A. (2006). Germline mutations in genes within the MAPK pathway cause cardio-facio-cutaneous syndrome. *Science* **311**, 1287-1290.

Sapkota, G., Alarcón, C., Spagnoli, F. M., Brivanlou, A. H. and Massagué, J. (2007). Balancing BMP signaling through integrated inputs into the Smad1 linker. *Mol. Cell* **25**, 441-454.

Sohn, S. J., Sarvis, B. K., Cado, D. and Winoto, A. (2002). ERK5 MAPK regulates embryonic angiogenesis and acts as a hypoxia-sensitive repressor of vascular endothelial growth factor expression. *J. Biol. Chem.* **277**, 43344-43351.

Song, B., Estrada, K. D. and Lyons, K. M. (2009). Smad signaling in skeletal development and regeneration. *Cytokine Growth Factor. Rev.* **20**, 379-388.

Takahata, Y., Hinoi, E., Takarada, T., Nakamura, Y., Ogawa, S. and Yoneda, Y. (2012). Positive regulation by gamma-aminobutyric acid B receptor subunit-1 of chondrogenesis through acceleration of nuclear translocation of activating transcription factor-4. *J. Biol. Chem.* **287**, 33293-33303.

Takarada, T., Nakazato, R., Tsuchikane, A., Fujikawa, K., Iezaki, T., Yoneda, Y. and Hinoi, E. (2016). Genetic analysis of Runx2 function during intramembranous ossification. *Development* **143**, 211-218.

Terpstra, L., Prud'homme, J., Arabian, A., Takeda, S., Karsenty, G., Dedhar, S. and St-Arnaud, R. (2003). Reduced chondrocyte proliferation and chondrodysplasia in mice lacking the integrin-linked kinase in chondrocytes. *J. Cell Biol.* **162**, 139-148.

Wang, L., Hinoi, E., Takemori, A., Takarada, T. and Yoneda, Y. (2005). Abolition of chondral mineralization by group III metabotropic glutamate receptors expressed in rodent cartilage. *Br. J. Pharmacol.* **146**, 732-743.

Wang, L., Mishina, Y. and Liu, F. (2015). Osterix-Cre transgene causes craniofacial bone development defect. *Calcif. Tissue Int.* **96**, 129-137.

Wang, C., Zhang, T., Liu, W., Meng, H., Song, Y. and Wang, W. (2016). Sox9-induced chondrogenesis in mesenchymal stem cells was mediated by ERK5 signal pathway. *Cell Mol. Biol.* **62**, 1-7.

Wu, Q., Huang, J. H., Sampson, E. R., Kim, K.-O. K., Zuscik, M. J., O'Keefe, R. J., Chen, D. and Rosier, R. N. (2009). Smurf2 induces degradation of GSK-3beta and upregulates beta-catenin in chondrocytes: a potential mechanism for Smurf2-induced degeneration of articular cartilage. *Exp. Cell Res.* **315**, 2386-2398.

Yan, L., Carr, J., Ashby, P. R., Murry-Tait, V., Thompson, C. and Arthur, J. S. C. (2003). Knockout of ERK5 causes multiple defects in placental and embryonic development. *BMC Dev. Biol.* **3**, 11.

Zhang, H. and Cohen, S. N. (2004). Smurf2 up-regulation activates telomere-dependent senescence. *Genes Dev.* **18**, 3028-3040.

Zhang, Y., Chang, C., Gehling, D. J., Hemmati-Brivanlou, A. and Derynck, R. (2001). Regulation of Smad degradation and activity by Smurf2, an E3 ubiquitin ligase. *Proc. Natl. Acad. Sci. USA* **98**, 974-979.

Zhou, G., Bao, Z. Q. and Dixon, J. E. (1995). Components of a new human protein kinase signal transduction pathway. *J. Biol. Chem.* **270**, 12665-12669.

DEVELOPMENT